HHS Public Access

Author manuscript

Cell Rep. Author manuscript; available in PMC 2016 March 24.

Published in final edited form as:

Cell Rep. 2015 March 24; 10(11): 1811–1818. doi:10.1016/j.celrep.2015.02.042.

XIRP2, an Actin-Binding Protein Essential for Inner Ear Hair-Cell Stereocilia

Déborah I. Scheffer[1,2], **Duan-Sun Zhang**[1], **Jun Shen**[1,3], **Artur Indzhykulian**[1], **K. Domenica Karavitaki**[1], **Yichao Joy Xu**[4], **Qinchuan Wang**[5], **Jim Jung-Ching Lin**[5], **Zheng-Yi Chen**[2], and **David P. Corey**[1]

[1]Department of Neurobiology and Howard Hughes Medical Institute, Harvard Medical School, Boston, MA - 02115

[2]Department of Otology and Laryngology, Harvard Medical School and Massachusetts Eye & Ear, Boston, MA - 02114

[3]Department of Pathology, Brigham and Women's Hospital, Harvard Medical School, Boston, MA - 02115

[4]Image and Data Analysis Core, Harvard Medical School, Boston, MA - 02115

[5]Department of Biology, University of Iowa, Iowa City, IA - 52242

SUMMARY

Hair cells of the inner ear are mechanoreceptors for hearing and balance, and proteins highly enriched in hair cells may have specific roles in the development and maintenance of the mechanotransduction apparatus. We identified XIRP2/mXinβ as an enriched protein likely to be essential for hair cells. We found that different isoforms of this protein are expressed and differentially located: short splice forms (also called XEPLIN) are targeted more to stereocilia, whereas two long isoforms containing a XIN-repeat domain are in both stereocilia and cuticular plates. Mice lacking the *Xirp2* gene developed normal stereocilia bundles, but these degenerated with time: stereocilia were lost and long membranous protrusions emanated from the nearby apical surfaces. At an ultrastructural level, the paracrystalline actin filaments became disorganized. XIRP2 is apparently involved in the maintenance of actin structures in stereocilia and cuticular plates of hair cells, and perhaps in other organs where it is expressed.

Contact Information: dcorey@hms.harvard.edu.

AUTHOR CONTRIBUTIONS

DIS, KDK, D-SZ, JS and AI performed experiments. YJX performed the image analysis. QW and JJ-CL made the *Xirp2*$^{-/-}$ strain and isoform-specific antibodies. DIS, Z-YC and DPC designed the studies and analyzed the data. DIS and DPC wrote the manuscript.

INTRODUCTION

Hair cells of the inner ear sense mechanical stimuli by deflection of a bundle of stereocilia extending from their apical surfaces, which leads to the opening of force-gated transduction channels at their tips. Each stereocilium has a stiff core of actin filaments in a paracrystalline array, maintained by actin crosslinking proteins such as plastin, fascin and espin, which allows stereocilia to pivot at their bases without bending along their lengths (Avenarius et al., 2014; Drenckhahn et al., 1991; Flock et al., 1982; Gillespie and Hudspeth, 1991; Karavitaki and Corey, 2010; Loomis et al., 2003; Shepherd et al., 1989; Shin et al., 2010; Tilney and DeRosier, 1986; Tilney et al., 1980; Tilney et al., 1989). The hair bundle is anchored into the cell body by actin rootlets that extend into the cuticular plate, a dense actin meshwork situated just below the apical surface. Each hair bundle also carries a single microtubule-based kinocilium, which is located at the periphery of the hair bundle adjacent to the tallest stereocilia and which extends from a cytoplasmic basal body through an actin-free hole in the cuticular plate termed the fonticulus. Microtubules and actin filaments, and their associated binding proteins, are essential for hair cell integrity and function.

XIRP2 (also known as CMYA3, myomaxin, or XIN beta) is a member of the actin-binding Xinrepeat-containing protein family (Duka et al., 2006; Okazaki et al., 2002; Pacholsky et al., 2004; Pan et al., 2003; Wang et al., 1996; Wang et al., 1999). The *Xirp2* gene is expressed in skeletal and cardiac muscle (Pan et al., 2003) and the protein has F-actin crosslinking activity through its 28 Xin domains (Cherepanova et al., 2006; Pacholsky et al., 2004). In muscle, XIRP2 localizes to the costameres and intercalated disks, two critical structural components of skeletal and cardiac muscle respectively (for review see (Jung-Ching Lin et al., 2005)).

A comparative analysis of the genes enriched in hair cells relative to other cell types indicated specific expression of *Xirp2* in hair cells, leading us to explore the function of the XIRP2 protein. Antibody labeling revealed it is a component of both the stereocilia and cuticular plates of hair cells. A mouse *Xirp2* knockout line exhibited a unique hair cell phenotype: the presence of very long membrane protrusions from the apical surface, the loss of regular actin filament spacing in the stereocilia, and the subsequent degeneration of stereocilia. XIRP2 is apparently an actinbinding protein required for the maintenance of actin filament structure in hair cells.

RESULTS

Xirp2 is expressed in mouse hair cells

From a hair-cell transcriptome study based on FACS purification of GFP-labeled hair cells (https://shield.hms.harvard.edu – GEO accession number GSE60019) we found that mouse *Xirp2*, encoding Xin-actin-binding-repeat-containing protein 2 (XIRP2), is highly enriched in hair cells and upregulated during mechanosensory development (Figure 1A). PCR amplification of cDNAs from FACS-purified hair cells at P4 confirmed the specificity of expression of *Xirp2* in hair cells (GFP+), with no detectable amplification in other cells of the sensory epithelium (GFP−) (Figure 1B).

Human *XIRP2* is Not Mutated in DFNB27

Many of the genes highly enriched in hair cells are deafness genes in humans and mice, so we asked whether *XIRP2* is a deafness gene as well. Although human *XIRP2* was first thought to be inside the DFNA16 locus (Fukushima et al., 1999), it was later excluded by testing other markers (Kasai et al., 2001). *XIRP2* remains within the DFNB27 locus (Pulleyn et al., 2000). We therefore sequenced the *XIRP2* exons and intron junctions in DNA from DFNB27-affected family members and healthy probands. We did not find any variant in *XIRP2* that segregated with hearing loss (data not shown), excluding this gene as a cause for DFNB27.

XIRP2 is a Component of Actin-Rich Structures in Mouse Hair Cells

XIRP2 is notable for its 28 Xin repeats, which bind and stabilize actin bundles (Pacholsky et al., 2004). We asked whether it is located at the actin-rich stereocilia and cuticular plates. Immunostaining for XIRP2 with an antibody (BSU2) raised against the Xin domains (Huang et al., 2006) revealed expression in inner hair cells (IHCs) and outer hair cells (OHCs) in the cochlea (Figure 1C), and in all hair cells of the vestibular system (Figure 1D). STED imaging showed that XIRP2 is localized throughout the actin-rich stereocilia and cuticular plates of both cochlear and utricular hair cells (Figure 1C, D – lower panels). Mice lacking XIRP2 lacked label in both stereocilia and cuticular plates (Figure 1E).

XIRP2 Isoforms Are Differentially Located

The *Xirp2* gene is expressed as six different splice forms, two long and four short (Figure 2A–C) (Wang et al., 2010). The conventional protein, known as XIRP2, is produced from two long splice forms containing 28 Xin repeats in a 3283 or 3784 amino-acid sequence (Figure 2B). Short splice forms produce proteins of 701 to 820 amino acids (Figure 2C). Sometimes termed XEPLINs, the short proteins lack Xin repeats and—because of a frame shift—have limited amino acid identity with long forms past exon 6. Shin *et al*. (2013) observed XIRP2 in chicken and rat stereocilia by mass spectroscopy, but found peptides corresponding only to the N and C termini and concluded that stereocilia contain only the short forms. From RNA-Seq data, we matched individual read sequences to specific exon sequences, and found that the Xin-repeatencoding exon 7 is indeed transcribed in hair cells (Figure S1). This was confirmed by RT-PCR: both the long forms of *Xirp2* including exon 7 (accession NM_001083919.1 and NM_001024618.2) and the short isoforms (accession EF119712.1, EF119713.1, EF119714.1, EF119715.1 and KM273012.1) are transcribed (Figure 2B, C). Finally, the BSU2 antibody in Figure 1 was raised against a peptide within the Xin-repeat domain (Huang et al., 2006), and it labeled stereocilia. At least one of the long forms is in stereocilia.

For further localization we used isoform-specific antibodies (Wang et al., 2010) (Figure 2D, E). In the cochlea, antibody U1043 (recognizing the short isoforms and long isoform 1) primarily labeled the hair bundles of IHCs and OHCs, with slight labeling of OHC cuticular plates (Figure 2D, top). The same was found in the crista, saccule (Figure 2D, bottom) and the utricle (data not shown), with labeling mostly near the bases of stereocilia. On the other hand, antibody U1040, recognizing long isoform 2, labeled IHC but not OHC cuticular plates and showed little or no labeling of hair bundles (Figure 2E, top panels). In the

vestibule, U1040 also failed to label hair bundles, but robustly labeled cuticular plates (in utricle) or pericuticular necklaces (in saccule) or both (in crista) (Figure 2E, bottom).

Based on U1040 staining, we conclude that long isoform 2 is generally in cuticular plates and pericuticular necklaces but not bundles. Based on the more widespread staining of BSU2 (recognizing both long isoforms; Figure 1) compared to that of U1040, we conclude that long isoform 1 is in hair bundles and possibly in cuticular plates. U1043 (recognizing short isoforms and long isoform 1) labels hair bundles; together with the mass spectrometry data from Shin *et al*. (2013), we conclude that XIRP2 short isoforms are in the hair bundles, but mostly not in cuticular plates.

Early Postnatal *Xirp2*$^{-/-}$ Hair Cells Have Normal Structure and Mechanotransduction

To understand the function of XIRP2, we investigated the function and morphology of the hair cells in *Xirp2/mXin*β knockout mice (strain *Xirp2*^{tm1Jl}, referred to here as *Xirp2*$^{-/-}$; (Wang et al., 2010)). These mice usually die in the third postnatal week (Wang et al., 2010), so we studied them before P16, precluding behavioral auditory or vestibular tests.

At P5, scanning electron microscopy (SEM) showed that *Xirp2*$^{-/-}$ hair cell morphology was grossly normal (data not shown). We then tested hair cell mechanotransduction with the fluorescent dye FM1–43, which is trapped in functional hair cells (Gale et al., 2001; Meyers et al., 2003). There was no noticeable difference in FM1–43 loading between control and *Xirp2*$^{-/-}$ hair cells in either cochlea or utricle (Figure S2A), suggesting normal transduction at P5. In cochlear hair cells dissected at P5 and cultured for two days, peak transduction current was not significantly different between control and *Xirp2*$^{-/-}$ mice (761 ± 63 pA compared to 723 ± 58 pA; mean ± SE; N=7 or 5) (Figure S2B). Both control and *Xirp2*$^{-/-}$ mice had prominent adaptation and there was no significant difference in its time constant.

Older *Xirp2*$^{-/-}$ Hair Cells Develop Long Apical Protrusions

At P7, some but not all *Xirp2*$^{-/-}$ mice showed short protrusions extending from OHC apical surfaces. These looked like kinocilium remnants because they were often situated at the fonticulus where the actin mesh of the cuticular plate is absent. By P11 they were often >10 μm, almost all hair cells had at least one and most had two, and they were situated throughout the apical surface around the bundle (Figures 3A and S3A,B). Such protrusions were never observed in control animals. Membrane protrusions were not labeled by phalloidin nor by acetylated tubulin antibody at P11 (Figure S3B) so they appear not to be related to either stereocilia or kinocilia. Instead they may be fluid-filled extensions of the apical membrane. Regardless of origin, their presence suggests disorganization of the cuticular plate.

Degeneration of OHC Kinocilia is Delayed in *Xirp2*$^{-/-}$ Mice

Cochlear hair cells lose their kinocilia from P5 to P10 in mice. However kinocilia in *Xirp2*$^{-/-}$ mice were retained for much longer. To reveal kinocilia clearly, we used an antibody to acetylated tubulin, labeling cochleas at P9 and P11 (Figure S3). In IHCs at P9, both control and *Xirp2*$^{-/-}$ hair cells retained kinocilia (0.9 ± 0.04 vs. 1.0 ± 0.0 kinocilia/cell respectively). OHCs lose kinocilia sooner than IHCs: control mice at P9 all lacked kinocilia,

from base to apex (0.0 ± 0.0 kinocilia/cell). At the same age, however, kinocilia persisted in most *Xirp2*$^{-/-}$ apical OHCs and in some middle turn OHCs (0.4 ± 0.16 kinocilia/cell overall). By P11, there were few if any acetylated-tubulin-labeled kinocilia remaining in either control or *Xirp2*$^{-/-}$ OHCs (Figure S3B), distinguishing lingering kinocilia from apical protrusions and indicating a developmental delay, in this aspect, of 2–3 days.

Xirp2$^{-/-}$ Mice Have Progressive Degeneration of Stereocilia

SEM of *Xirp2*$^{-/-}$ mice also revealed a progressive degeneration of the shortest row of stereocilia in OHCs, and stunted or missing stereocilia in IHC bundles. The stereocilia loss occurred as early as P9 at the base (data not shown) and had progressed to the middle turn by P11 and P13 (Figure 3B, C). In addition, the tallest row of IHC stereocilia were 5–10% thinner in the *Xirp2*$^{-/-}$ mice at both P11 and P13 (Figure 3D). On the other hand, the tallest row of OHC stereocilia were slightly thicker (Figure 3D), suggesting a general dysregulation of stereocilia actin bundling in the absence of XIRP2.

Three-dimensional renderings of hair bundles, labeled with an antibody to the cell-surface protein PMCA2 and a phalloidin counterstain for actin (not shown), revealed a slight shortening of OHC stereocilia in *Xirp2*$^{-/-}$ mice (Figure 3E). At P5, the height difference was larger at the base and middle turn than at the apex, consistent with a developmental progression of the shortening from base to apex.

The Paracrystalline Array of Stereocilia Actin is Disorganized in *Xirp2* Knockouts

The SEM beam often caused curling of *Xirp2*$^{-/-}$ stereocilia (Figure S4C), which did not occur in controls or with additional osmium fixation. We used transmission electron microscopy (TEM) to investigate further the ultrastructure of the actin in stereocilia. At P7, the overall morphology of *Xirp2*$^{-/-}$ stereocilia was normal: the membrane was similar to controls, and the rootlets were present (Figure 4A). In control animals, actin filaments were organized in a paracrystalline array with highly regular filament spacing over tens of nanometers. In *Xirp2*$^{-/-}$ stereocilia, however, filament spacing was less regular, with numerous gaps and disordered regions (Figure 4A, see insets and brackets). These ultrastructural abnormalities were observed in both IHCs and OHCs from both the base and apex of the cochlea, and in vestibular hair cells. They were more pronounced in basal IHCs. Similar results were obtained at P16 (data not shown).

To quantify the disorganization, we first used an autocorrelation function on TEM images of stereocilium cores, in a direction perpendicular to the long axis of the stereocilium. The autocorrelation for control stereocilia usually revealed regular filament spacing, observed as a ripple pattern extending in either direction from zero. An example, from an apical IHC, is shown in Figure 4B (blue); autocorrelation analysis showed average spacing of 9.9 nm (not corrected for shrinkage). In contrast, an image from the same region of a *Xirp2*$^{-/-}$ cochlea showed no ripple, indicating a lack of regular filament spacing (Figure 4B, red).

We then used a Fourier transform on many images of stereocilia to quantify the degree of periodicity in the filament spacing along the same axis. Figures 4C–E show the spectral density of TEM images, represented on a wavelength scale. Figure 4D, for instance,

represents the averaged Fourier transforms of 19 apical IHC stereocilia. Control stereocilia have a peak at about 9.2 nm, in agreement with the autocorrelation function. Notably, however, the *Xirp2*$^{-/-}$ stereocilia showed a peak shifted to greater spacing, in this case to about 11 nm. In all cases, *Xirp2*$^{-/-}$ stereocilia showed longer spacing. This was observed also at P16 (data not shown). Both the broadened interfilament spacing and the regions of absent filaments in some TEM images are consistent with a role for XIRP2 in maintaining crosslinked actin filaments in stereocilia.

DISCUSSION

Expression of the actin-binding protein XIRP2 was highly enriched in utricular and cochlear hair cells and increased markedly after E16, suggesting an important role in the actin-rich hair bundles. Antibody labeling indeed showed that XIRP2 is located in both stereocilia and cuticular plates of mouse cochlear and utricular hair cells. These results confirm and extend the findings of Shin *et al*. (2013) in chicken and rat.

XIRP2 might serve to cross-link actin filaments in stereocilia. Three Xin repeats can bind one actin molecule (Pacholsky et al., 2004), so each XIRP2 long-isoform molecule, containing 28 Xin repeats, could bind multiple actin filaments. Similarly, full-length mouse XIRP1 has actin bundling activity, crosslinking filaments into parallel arrays (Choi et al., 2007).

However, isoform-specific antibodies revealed that long isoform 2 is primarily in the cuticular plate and pericuticular necklace, and short isoforms are almost exclusively in the hair bundle. Long isoform 1 is also in hair bundle but is mostly near the base in vestibular hair cells; it may also be in cuticular plates.

Based on mass spectrometry analysis, short-form XIRP2 is an abundant protein of chicken stereocilia (Avenarius et al., 2014; Shin et al., 2013). An average stereocilium with 400,000 actin monomers has ~4,600 XIRP2 short isoform molecules (Shin et al., 2013). There is therefore one XIRP2 short form for ~87 actin monomers; if spaced evenly in stereocilia, they are ~260 nm apart. Based on 210 actin filaments in a chick stereocilium (Shin et al., 2013), there are 22 XIRP2 short form molecules per full-length filament. Both the long isoform1 and the short isoforms are predicted to include a LIM domain (http://prosite.expasy.org/). In cardiomyocytes, Muscle LIM Protein self-associates with one of its LIM domains and binds actin filaments with another (Hoffmann et al., 2014). Thus XIRP2 short isoforms may interact with each other and bind actin filaments.

At the same time, the actin crosslinker FASCIN2—present at ~40,000 copies per stereocilium or almost 200 molecules per filament (Shin et al., 2013)—is much more abundant and so is likely to be the major crosslinking protein. XIRP2 may thus have a more specialized role.

Xirp2$^{-/-}$ mice exhibited an unprecedented phenotype in hair cells: the loss of the actin paracrystalline array in the stereocilia followed by their progressive degeneration. This was observed most strikingly in the Fourier transforms of electron micrographs, where the regular spacing of actin filaments was disrupted. Stereocilia in most hair cells were also

slightly shorter and thinner by the second postnatal week. This phenotype is most consistent with a role for XIRP2 in stereocilia that involves protection or repair of the actin structure.

Actin maintenance and repair are critical for cells like hair cells and cardiac myocytes that are replaced slowly if at all during life. We previously tagged newly synthesized proteins with ^{15}N and detected it within hair cells using multi-isotope imaging mass spectroscopy (Zhang et al., 2012). Stereocilia proteins displayed a remarkably low turnover rate, with less than 50% replacement in two months, and there was no evidence of replacement of actin by treadmilling. Thus there is not an obvious mechanism to repair breaks caused by noise trauma or aging (Belyantseva et al., 2009). It may be that actin filaments polymerize and depolymerize at multiple locations along the length of a stereocilium (Zhang et al., 2012). Perhaps XIRP2, binding at a filament end, normally protects from depolymerization and the *Xirp2*$^{-/-}$ phenotype results from an imbalance that allows filaments to shorten within a stereocilium, producing gaps. Indeed, Pacholsky *et al*. (2004) showed that the binding of Xin repeats to actin filaments protects F-actin from depolymerization.

Or perhaps XIRP2 is a staging protein that allows broken filaments to re-anneal, and they fail to do so in the knockout. Either way, the paracrystalline array, height and thickness of the stereocilia determine the mechanical properties of the hair bundles, and a change of these properties could affect their function in hearing. We were unable to test the hearing of the *Xirp2*$^{-/-}$ mice, as they die before P17 (Wang et al., 2010). We expect, however, that the disintegration and loss of stereocilia would lead to a progressive hearing loss if the mice survived, which might be tested with a conditional deletion of XIRP2 in hair cells. Although we did not find *XIRP2* mutations in DFNB27 patients, this gene remains a good candidate for deafness in humans.

The other striking phenotype of *Xirp2*$^{-/-}$ mice was the development of long protrusions from the cuticular plate. These appeared not to contain either actin or microtubules and their genesis is unclear. In *Xirp2*$^{-/-}$ mice, the F-actin meshwork of the cuticular plates might be looser or the failure of membrane-cytoskeletal adhesion may allow the extrusion of membrane from weaker spots in the apical surface. A similar phenotype was described in Tmprss3^{Y260X} mutant mice (Fasquelle et al., 2011) although the protrusions were reported to be kinocilia.

In both stereocilia and cuticular plates of hair cells, XIRP2 seems to be involved in the protection or repair of actin filament structures. It may play a similar roles in the other tissues—most importantly cardiac and skeletal muscle—where it is expressed.

EXPERIMENTAL PROCEDURES

Animal Protocols

All experiments were carried out in compliance with ethical regulations and approved by the Animal Care Committees of the Massachusetts Eye & Ear and Harvard Medical School.

RT-PCR

RNA was extracted from P6 cochleas, utricles and hearts of CD1 mice using QIAzol (Qiagen), treated with DNAseI (Roche), and reverse-transcribed with Superscript II (Invitrogen) to generate cDNA. PCR reactions were performed with recombinant Taq DNA polymerase (Invitrogen). Primers used are in the Supplemental Experimental Procedures.

FM1–43 Dye Accumulation

Mouse utricles and cochleas (P5) were gently dissected and treated with 5 μ M FM1–43 (Invitrogen) for 20 seconds, then washed for 2 min. Tissues treated with FM1–43 were then viewed with a confocal microscope (Olympus Fluoview 1000). Images shown are maximum value projections of FM1–43 fluorescence stacks.

Electrophysiology

OHC mechanotransduction current recordings were done using the conventional whole cell patch clamp technique. Cultured organ of Corti explants (P5+2–3 days *in vitro*) were observed with an inverted microscope (Nikon TE2000 with 100× 1.3NA objective) and the middle part of the OC explant used in all cases. Both, intracellular and extracellular solutions, as well as the experimental arrangement were used as described previously (Indzhykulian et al., 2013). Hair cell bundles were stimulated with glass probe mounted on a piezo stack actuator driven by custom made driver amplifier to deliver a family of stepwise stimuli of increased amplitude. Stimulus protocol was low-pass filtered at 20 kHz frequency.

Immunohistochemistry

Inner ears of P6 CD1, control (*Xirp2*$^{+/+}$ or *Xirp2*$^{+/-}$) or *Xirp2*$^{-/-}$ littermate mice were collected, fixed in 4% paraformaldehyde. A microwave antigen retrieval technique was applied (H-3300, Vector Laboratories) on cryosections prior to permeabilization/ blocking in 1X PBS + 0.05% triton (0.3% for whole mount) + 8% normal goat serum for 1 h at room temperature. The sections/tissues were then incubated with primary antibodies overnight at 4°C and secondary antibodies for 1 h in blocking solution at room temperature. Stained slices and tissues were mounted with ProLong Gold or Diamond Antifade Reagent with DAPI (Invitrogen). Antibodies used can be found in the Supplemental Experimental Procedures. Samples were imaged on a confocal microscope (Olympus Fluoview 1000) or a Super-Resolution Leica TCS STED followed by Huygens deconvolution.

Scanning electron microscopy

Whole inner ears were excised and fixed in 2.5% (vol/vol) glutaraldehyde in 0.1 M sodium cacodylate buffer containing 2 mM calcium chloride (pH 7.4). When necessary (after P10), the inner ears were decalcified in EDTA (125 mM, pH 8). The cochleas were then dissected to expose the organ of Corti and prepared as previously described (Jagger et al., 2014). Observations were made on a Hitachi S4800 field-emission scanning electron microscope.

Transmission electron microscopy

Tissues were harvested, fixed and dissected as for SEM. Tissues were then processed and imaged as previously described (Karavitaki and Corey, 2010).

The images were analyzed by using two sets of custom functions created in MATLAB (MathWorks) along with a software suite created for automated file sorting and regions of interest cropping. Details in Supplemental Experimental Procedures.

Stereocilia length and width measurements

Whole mount cochleas were labeled with phalloidin and with an antibody to PMCA2. Imaris software (Bitplane AG) was used to convert confocal images into three-dimensional renderings, and a custom MATLAB script calculated the stereocilia lengths. SEM images were analyzed in ImageJ (NIH). Statistical analyses used two-tailed T-tests in GraphPad Prism (GraphPad Software).

Supplementary Material

Refer to Web version on PubMed Central for supplementary material.

ACKNOWLEDGEMENTS

We appreciate help with FM1–43 loading from Paul Niksch at Harvard Medical School, help with initial ABR tests on another XIRP2 mutant from Sharon Kujawa at Massachusetts Eye & Ear, advice on image analysis from Hunter Elliott and Tiao Xie at the Harvard Medical School Image and Data Analysis Core, and electron microscopy support from Louise Trakimas at Harvard Medical School and William Fowle at Northeastern University. We appreciate a PMCA2 antibody from Peter Barr-Gillespie at Oregon Health & Science University, and a XIRP2 antibody from Francisco Naya at Boston University. We thank Andy Sharpe and Chris Bennet at the University of Leeds (UK) for providing us with the DFNB27 family DNAs. We thank the Harvard Neurobiology Imaging Facility (a part of the Neural Imaging Center supported by NINDS P30 Core Center grant NS072030) for consultation and instrumentation. This research was supported by NIH grants R01-DC000304 and R01-DC002281 (to DPC), R01-DC006908 (to ZYC), P30-DC05209 to the Massachusetts Eye & Ear, RO1-HL107383 (to JJ-CL) and by a Frederick and Ines Yeatts Hair Cell Regeneration grant (to Z-YC). DPC is an Investigator, and KDK and D-SZ were Associates of the Howard Hughes Medical Institute. We thank Dr. Lisa Goodrich for helpful comments on the manuscript.

References

Avenarius MR, Saylor KW, Lundeberg MR, Wilmarth PA, Shin JB, Spinelli KJ, Pagana JM, Andrade L, Kachar B, Choi D, et al. Correlation of actin crosslinker and capper expression levels with stereocilia growth phases. Mol Cell Proteomics. 2014; 13:606–620. [PubMed: 24319057]

Belyantseva IA, Perrin BJ, Sonnemann KJ, Zhu M, Stepanyan R, McGee J, Frolenkov GI, Walsh EJ, Friderici KH, Friedman TB, Ervasti JM. Gamma-actin is required for cytoskeletal maintenance but not development. Proc Natl Acad Sci U S A. 2009; 106:9703–9708. [PubMed: 19497859]

Cherepanova O, Orlova A, Galkin VE, van der Ven PF, Furst DO, Jin JP, Egelman EH. Xin-repeats and nebulin-like repeats bind to F-actin in a similar manner. J Mol Biol. 2006; 356:714–723. [PubMed: 16384582]

Choi S, Gustafson-Wagner EA, Wang Q, Harlan SM, Sinn HW, Lin JL, Lin JJ. The intercalated disk protein, mXinalpha, is capable of interacting with beta-catenin and bundling actin filaments [corrected]. J Biol Chem. 2007; 282:36024–36036. [PubMed: 17925400]

Drenckhahn D, Engel K, Hofer D, Merte C, Tilney L, Tilney M. Three different actin filament assemblies occur in every hair cell: each contains a specific actin crosslinking protein. J Cell Biol. 1991; 112:641–651. [PubMed: 1993735]

Duka A, Schwartz F, Duka I, Johns C, Melista E, Gavras I, Gavras H. A Novel Gene (Cmya3) Induced in the Heart by Angiotensin II-Dependent but not Salt-Dependent Hypertension in Mice. Am J Hypertens. 2006; 19:275–281. [PubMed: 16500513]

Fasquelle L, Scott HS, Lenoir M, Wang J, Rebillard G, Gaboyard S, Venteo S, Francois F, Mausset-Bonnefont AL, Antonarakis SE, et al. Tmprss3, a transmembrane serine protease deficient in human

DFNB8/10 deafness, is critical for cochlear hair cell survival at the onset of hearing. J Biol Chem. 2011; 286:17383–17397. [PubMed: 21454591]

Flock A, Bretscher A, Weber K. Immunohistochemical localization of several cytoskeletal proteins in inner ear sensory and supporting cells. Hear Res. 1982; 7:75–89. [PubMed: 6178719]

Fukushima K, Kasai N, Ueki Y, Nishizaki K, Sugata K, Hirakawa S, Masuda A, Gunduz M, Ninomiya Y, Masuda Y, et al. A gene for fluctuating, progressive autosomal dominant nonsyndromic hearing loss, DFNA16, maps to chromosome 2q23–24.3. Am J Hum Genet. 1999; 65:141–150. [PubMed: 10364526]

Gale JE, Marcotti W, Kennedy HJ, Kros CJ, Richardson GP. FM1–43 dye behaves as a permeant blocker of the hair-cell mechanotransducer channel. J Neurosci. 2001; 21:7013–7025. [PubMed: 11549711]

Gillespie PG, Hudspeth AJ. High-purity isolation of bullfrog hair bundles and subcellular and topological localization of constituent proteins. J Cell Biol. 1991; 112:625–640. [PubMed: 1704375]

Hoffmann C, Moreau F, Moes M, Luthold C, Dieterle M, Goretti E, Neumann K, Steinmetz A, Thomas C. Human muscle LIM protein dimerizes along the actin cytoskeleton and cross-links actin filaments. Mol Cell Biol. 2014; 34:3053–3065. [PubMed: 24934443]

Huang HT, Brand OM, Mathew M, Ignatiou C, Ewen EP, McCalmon SA, Naya FJ. Myomaxin is a novel transcriptional target of MEF2A that encodes a Xin-related alpha-actinin-interacting protein. J Biol Chem. 2006; 281:39370–39379. [PubMed: 17046827]

Indzhykulian AA, Stepanyan R, Nelina A, Spinelli KJ, Ahmed ZM, Belyantseva IA, Friedman TB, Barr-Gillespie PG, Frolenkov GI. Molecular remodeling of tip links underlies mechanosensory regeneration in auditory hair cells. PLoS Biol. 2013; 11:e1001583. [PubMed: 23776407]

Jagger DJ, Nickel R, Forge A. Gap junctional coupling is essential for epithelial repair in the avian cochlea. J Neurosci. 2014; 34:15851–15860. [PubMed: 25429127]

Jung-Ching Lin J, Gustafson-Wagner EA, Sinn HW, Choi S, Jaacks SM, Wang DZ, Evans S, Li-Chun Lin J. Structure, Expression, and Function of a Novel Intercalated Disc Protein, Xin. J Med Sci. 2005; 25:215–222. [PubMed: 16708114]

Karavitaki KD, Corey DP. Sliding adhesion confers coherent motion to hair cell stereocilia and parallel gating to transduction channels. J Neurosci. 2010; 30:9051–9063. [PubMed: 20610739]

Kasai N, Fukushima K, Ueki Y, Prasad S, Nosakowski J, Sugata K, Sugata A, Nishizaki K, Meyer NC, Smith RJ. Genomic structures of SCN2A and SCN3A - candidate genes for deafness at the DFNA16 locus. Gene. 2001; 264:113–122. [PubMed: 11245985]

Loomis PA, Zheng L, Sekerkova G, Changyaleket B, Mugnaini E, Bartles JR. Espin cross-links cause the elongation of microvillus-type parallel actin bundles in vivo. J Cell Biol. 2003; 163:1045–1055. [PubMed: 14657236]

Meyers JR, MacDonald RB, Duggan A, Lenzi D, Standaert DG, Corwin JT, Corey DP. Lighting up the senses: FM1–43 loading of sensory cells through nonselective ion channels. J Neurosci. 2003; 23:4054–4065. [PubMed: 12764092]

Okazaki Y, Furuno M, Kasukawa T, Adachi J, Bono H, Kondo S, Nikaido I, Osato N, Saito R, Suzuki H, et al. Analysis of the mouse transcriptome based on functional annotation of 60,770 full-length cDNAs. Nature. 2002; 420:563–573. [PubMed: 12466851]

Pacholsky D, Vakeel P, Himmel M, Lowe T, Stradal T, Rottner K, Furst DO, van der Ven PF. Xin repeats define a novel actin-binding motif. J Cell Sci. 2004; 117:5257–5268. [PubMed: 15454575]

Pan PW, Li K, Tuggle CK, Yu M, Liu B, Zhao SH. Sequencing, tissue distribution and physical mapping of the porcine homologue of cardiomyopathy associated 3 (CMYA3). Anim Genet. 2003; 34:473–474. [PubMed: 14687087]

Pulleyn LJ, Jackson AP, Roberts E, Carridice A, Muxworthy C, Houseman M, Al-Gazali LI, Lench NJ, Markham AF, Mueller RF. A new locus for autosomal recessive non-syndromal sensorineural hearing impairment (DFNB27) on chromosome 2q23–q31. Eur J Hum Genet. 2000; 8:991–993. [PubMed: 11175289]

Shepherd GM, Barres BA, Corey DP. "Bundle blot" purification and initial protein characterization of hair cell stereocilia. Proc Natl Acad Sci U S A. 1989; 86:4973–4977. [PubMed: 2662191]

Shin JB, Krey JF, Hassan A, Metlagel Z, Tauscher AN, Pagana JM, Sherman NE, Jeffery ED, Spinelli KJ, Zhao H, et al. Molecular architecture of the chick vestibular hair bundle. Nat Neurosci. 2013; 16:365–374. [PubMed: 23334578]

Shin JB, Longo-Guess CM, Gagnon LH, Saylor KW, Dumont RA, Spinelli KJ, Pagana JM, Wilmarth PA, David LL, Gillespie PG, Johnson KR. The R109H variant of fascin-2, a developmentally regulated actin crosslinker in hair-cell stereocilia, underlies early-onset hearing loss of DBA/2J mice. J Neurosci. 2010; 30:9683–9694. [PubMed: 20660251]

Tilney LG, DeRosier DJ. Actin filaments, stereocilia, and hair cells of the bird cochlea. IV. How the actin filaments become organized in developing stereocilia and in the cuticular plate. Dev Biol. 1986; 116:119–129. [PubMed: 3732602]

Tilney LG, Derosier DJ, Mulroy MJ. The organization of actin filaments in the stereocilia of cochlear hair cells. J Cell Biol. 1980; 86:244–259. [PubMed: 6893452]

Tilney MS, Tilney LG, Stephens RE, Merte C, Drenckhahn D, Cotanche DA, Bretscher A. Preliminary biochemical characterization of the stereocilia and cuticular plate of hair cells of the chick cochlea. J Cell Biol. 1989; 109:1711–1723. [PubMed: 2677026]

Wang DZ, Hu X, Lin JL, Kitten GT, Solursh M, Lin JJ. Differential displaying of mRNAs from the atrioventricular region of developing chicken hearts at stages 15 and 21. Front Biosci. 1996; 1:a1–a15. [PubMed: 9159189]

Wang DZ, Reiter RS, Lin JL, Wang Q, Williams HS, Krob SL, Schultheiss TM, Evans S, Lin JJ. Requirement of a novel gene, Xin, in cardiac morphogenesis. Development. 1999; 126:1281–1294. [PubMed: 10021346]

Wang Q, Lin JL, Reinking BE, Feng HZ, Chan FC, Lin CI, Jin JP, Gustafson-Wagner EA, Scholz TD, Yang B, Lin JJ. Essential roles of an intercalated disc protein, mXinbeta, in postnatal heart growth and survival. Circ Res. 2010; 106:1468–1478. [PubMed: 20360251]

Zhang DS, Piazza V, Perrin BJ, Rzadzinska AK, Poczatek JC, Wang M, Prosser HM, Ervasti JM, Corey DP, Lechene CP. Multi-isotope imaging mass spectrometry reveals slow protein turnover in hair-cell stereocilia. Nature. 2012; 481:520–524. [PubMed: 22246323]

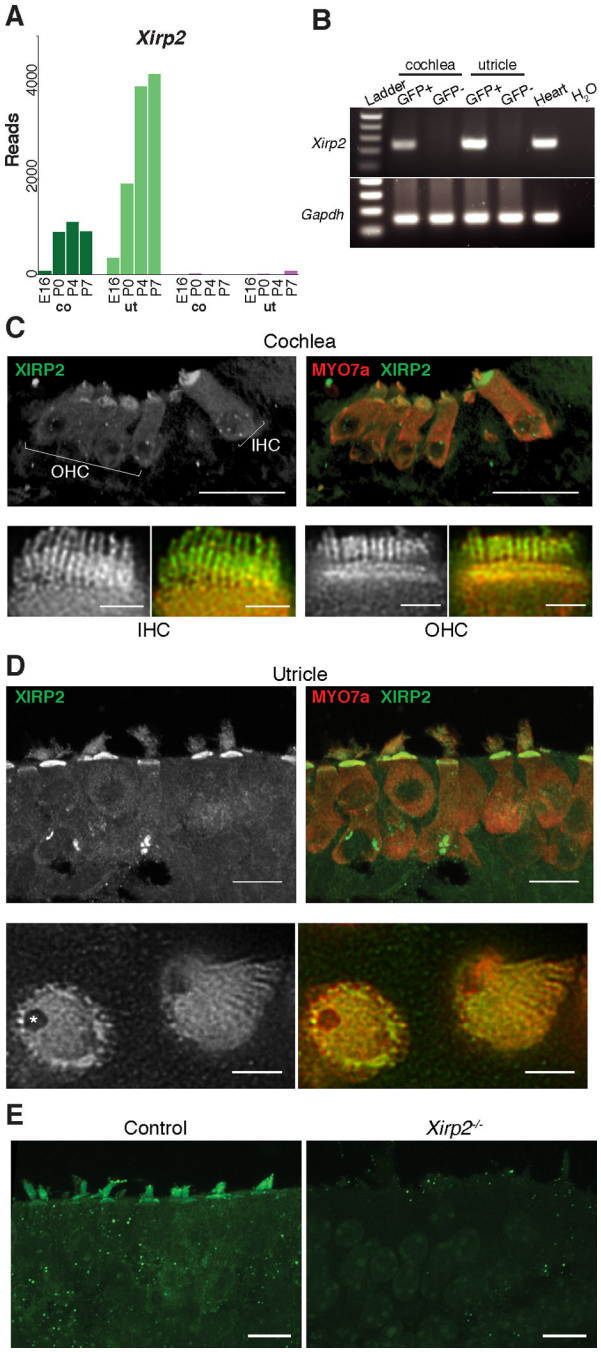

Figure 1. *Xirp2* is Expressed in Hair Cells

(A) RNA-Seq read counts for *Xirp2*. Expression was detected in hair cells (green bars), and increased after age E16 in cochlea (co) and utricle (ut). Expression in other cell types (purple bars) was much lower, about 4% that in hair cells.

(B) Confirmation of *Xirp2* expression in P4 FACS samples by RT-PCR. *Xirp2* was amplified only in hair cell (GFP+) samples from the inner ear. Heart provided a positive control.

(C) Antibody (BSU2) labeling of XIRP2 long isoforms in P6 cochlear hair cells. Upper panels are confocal images (scale bars = 20 μm) and lower panels are STED images of cryosections, showing inner hair cells (IHC) and outer hair cells (OHC) (scale bars = 2 μm). XIRP2 long isoforms are concentrated in the cuticular plate and hair bundle.
(D) Antibody labeling of XIRP2 long isoforms in P6 saccule. XIRP2 is concentrated in the cuticular plate and hair bundle and absent in the fonticulus (*).
(E) Immunoreactivity is absent in *Xirp2* knockout mice utricle, validating the antibody.

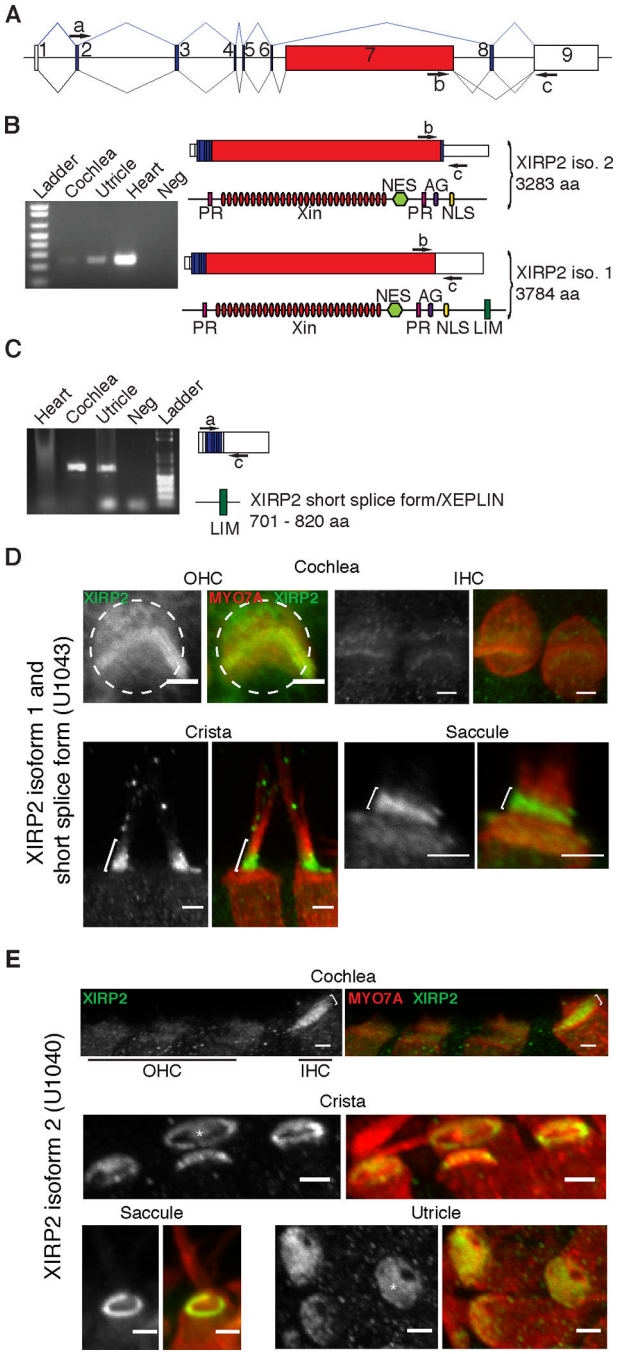

Figure 2. Long and Short Isoforms of *Xirp2* Are Expressed in the Inner Ear and Have Differential Localization In Hair Cells

(A) Schematic of the *Xirp2* gene structure. White boxes represent long-isoform non-coding or partially coding exons, blue boxes are coding exons and red indicates the Xin-domain-encoding exon 7. PCR primers a-c are indicated.

(B) RT-PCR on cochlea, utricle and heart. The product of primers b and c shows the expression of XIRP2 long forms, which carry 28 Xin repeats (red ovals), two proline-rich regions (PR), a Leu-rich nuclear export signal (NES), a bipartite nuclear localization signal

profile (NLS) and an ATP/GTP-binding site motif A (AG). When exon 8 is retained in isoform 2, the corresponding XIRP2 protein is 3283 amino acids long. When exon 8 is spliced out in isoform 1, it creates a frameshift that leads to a longer protein (3784 amino acids), which includes the LIM domain.

(C) The product of primers a and c shows the expression of splice forms encoding XIRP2 short isoforms (XEPLIN) in cochlea and utricle. Short forms carry a LIM domain (green) absent in the long isoform 2.

(D) Antibody (U1043) labeling of XIRP2 long isoform 1 and short isoforms in P6 hair cells. In OHCs, U1043 label was in cuticular plate (dashed circle) but primarily in stereocilia. In IHCs, U1043 label was mainly detected in the stereocilia. In vestibular system, U1043 label was found in stereocilia, with a stronger signal at the base of stereocilia (brackets), and less so in the cuticular plate of saccular hair cells.

(E) Antibody (U1040) labeling of XIRP2 isoform 2 in P6 hair cells. In the cochlea, there was a strong signal in IHCs cuticular plate (brackets) and little or no expression in OHCs. In vestibular system, XIRP2 isoform 2 was detected at the pericuticular necklace of crista and saccule hair cells, and in the cuticular plate (*) of utricular and crista hair cells. (scale bars = 2 μm)

See also Figure S1.

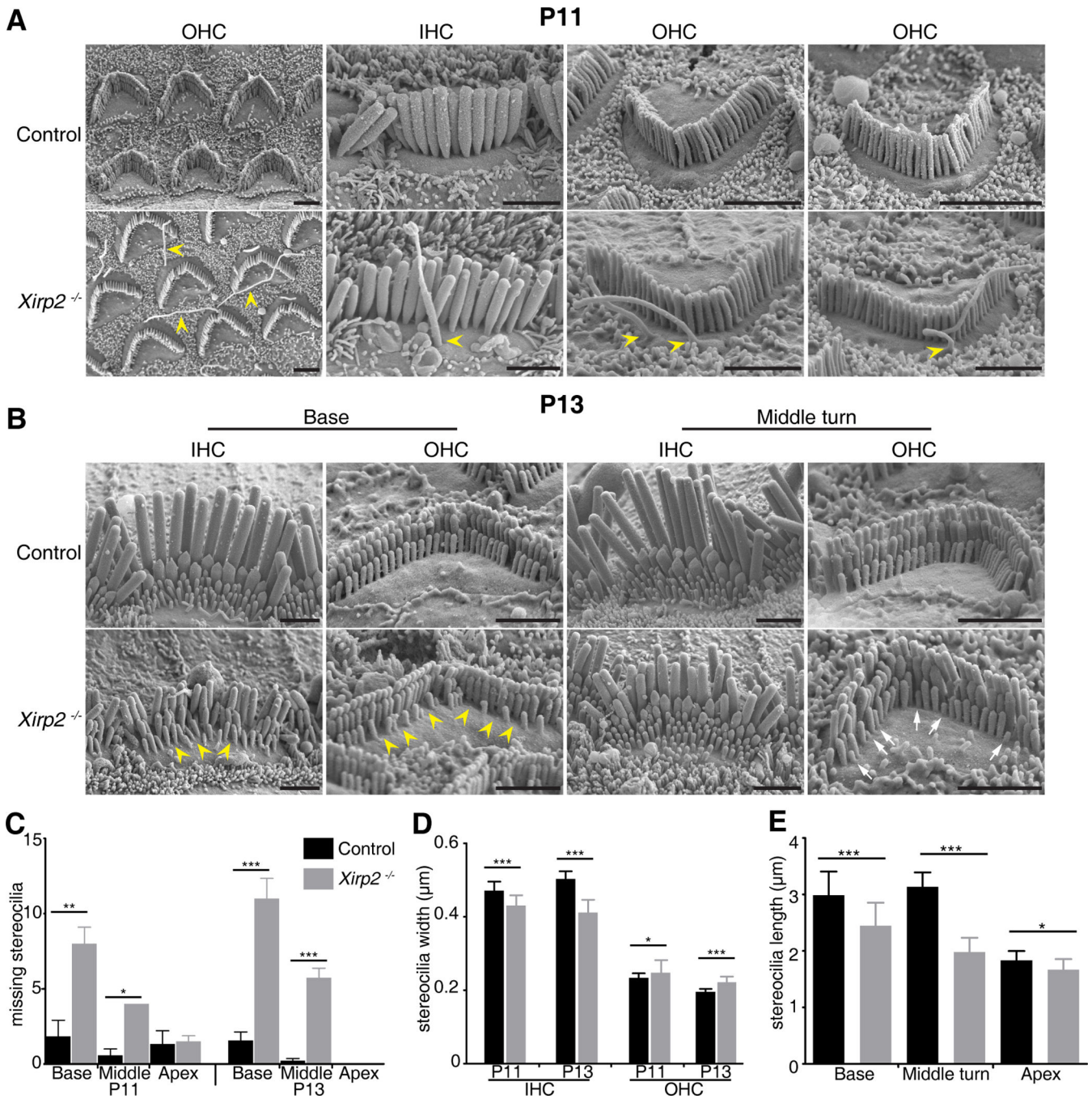

Figure 3. Cell Surface and Stereocilia Defects in *Xirp2*$^{-/-}$ Mice

(A) SEM images of P11 *Xirp2*$^{-/-}$ cochlear hair cells. Note the presence of multiple long membrane protrusions at the apical surfaces of *Xirp2*$^{-/-}$ hair cells (yellow arrowheads).

(B) SEM images at P13 showed loss (yellow arrow heads) or shortening (white arrows) of some stereocilia in *Xirp2*$^{-/-}$ mice. Scale bar = 2 µ m.

(C) Missing OHC stereocilia at P11 and P13, at the base, middle and apex of the cochlea, determined from SEM images. Mean ± SEM. *p*-value calculated by Student's t-test. * p<0.05; *** p<0.0005

(D) Stereocilia widths in the tallest row of IHCs and OHCs at P11 and P13. *Xirp2*$^{-/-}$ stereocilia are thinner than wildtype in IHCs but slightly wider in OHCs. Mean ± SD.
(E) Stereocilia lengths measured at P5 in OHCs, from 3D confocal imaging of cochleas labeled with an antibody to PMCA2. Hair cells lacking XIRP2 have shorter stereocilia. Mean ± SD.
See also Figures S2, S3 and S4.

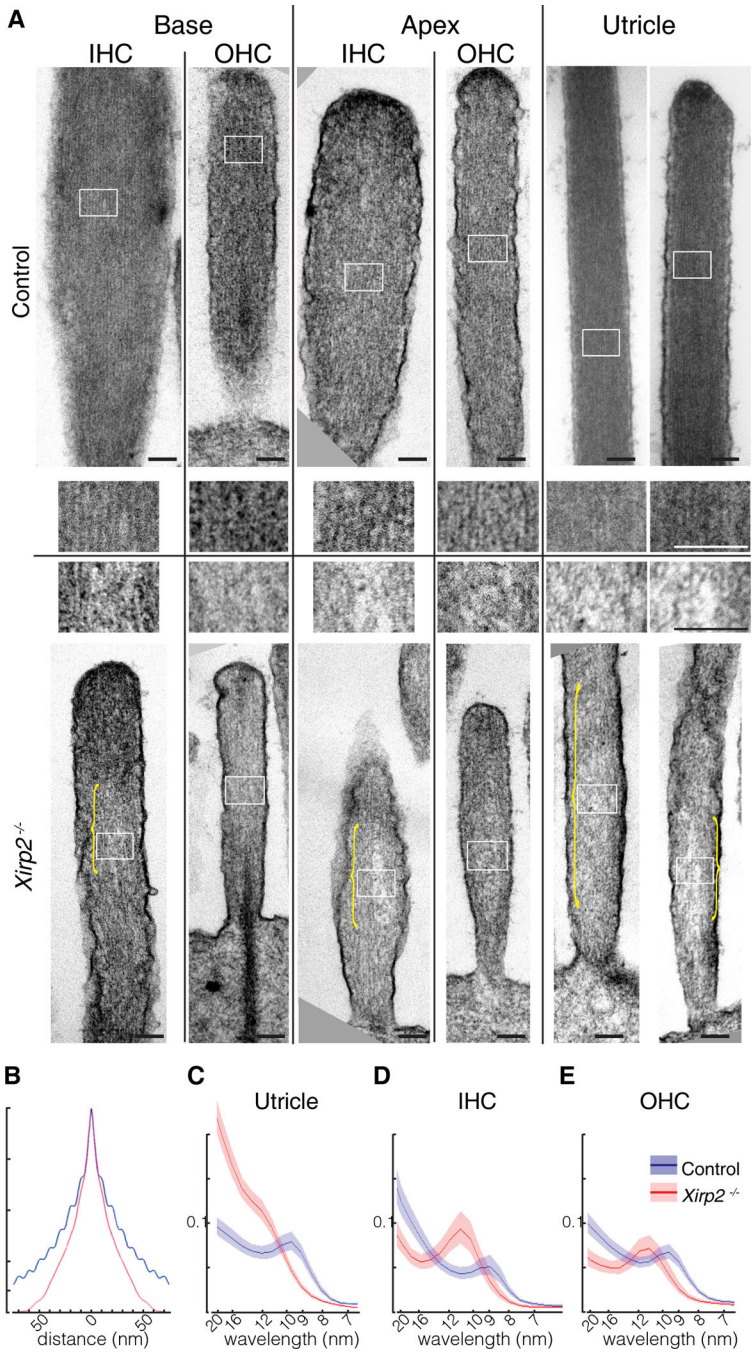

Figure 4. Disruption of Paracrystalline Actin Cores in *Xirp2*$^{-/-}$ Stereocilia

(A) TEM images of control and *Xirp2*$^{-/-}$ stereocilia in basal and apical turns of the cochlea and in utricle, at P7. Upper panels are control; lower panels are knockout. Insets for each (white boxes) are shown at a higher magnification in the middle. Note the disorganization of actin filaments in *Xirp2*$^{-/-}$ stereocilia (yellow brackets). Scale bars = 100 nm.

(B) Autocorrelation function for TEM images of stereocilia cores of apical IHCs at P7, in the direction perpendicular to the actin filaments. Blue is from a control mouse (27

stereocilia); red is from a *Xirp2*$^{-/-}$ mouse (24 stereocilia). The ripple pattern reflects the regular spacing of actin filaments at about 10 nm.

(C) Averaged Fourier transforms of TEM images from utricle stereocilia (14 control images, 20 *Xirp2*$^{-/-}$ images). Control stereocilia (blue) showed a clear peak at about 10 nm; *Xirp2*$^{-/-}$ stereocilia (red) had wider and less regular spacing. Lighter red and blue lines represent confidence interval of the Fourier transforms.

(D) Fourier transforms of P7 IHCs (9 control and 4 *Xirp2*$^{-/-}$ images).

(E) Fourier transforms of P7 OHCs (20 control and 8 *Xirp2*$^{-/-}$ images).